DOI: 10.17725/rensit.2020.12.253

Inverse problems of macrofracture formations exploration seismology solution with use of convolutional neural networks

Maxim V. Muratov, Vasily V. Ryazanov, Igor B. Petrov

Moscow Institute of Physics and Technology, https://mipt.ru
Dolgoprudnyi 141700, Moscow region, Russian Federation

E-mail: max.muratov@gmail.com, vassavadda@gmail.com, petrov@mipt.ru

Received July 3, 2020, peer reviewed July 07, 2020, accepted July 08, 2020

Abstract. **This article is devoted to solving the inverse problems of exploration seismology of uniformly oriented macrofractures systems using convolutional neural networks. The use of convolutional neural networks is optimal due to the multidimensionality of the studied data object. A training sample was formed using mathematical modeling. In the numerical solution of direct problems, a grid-characteristic method with interpolation on unstructured triangular meshes was used to form a training sample. The grid-characteristic method most accurately describes the dynamic processes in exploration seismology problems, since it takes into account the nature of wave phenomena. The approach used makes it possible to construct correct computational algorithms at the boundaries and contact boundaries of the integrational domain. Fractures were set discretely in the integration domain in the form of boundaries and contact boundaries. The article presents the results of solving inverse problems with variations in the angle of inclination of fractures, height of fractures, density of fractures in the system, as well as joint variations in the angle of inclination and height of fractures and all three investigated parameters.**

Keywords: **machine learning, convolutional neural networks, mathematical modeling, grid-characteristic method, exploration seismology, inverse problems, fractured media**

UDC 004.93

Acknowledgments. This work was carried out as part of the RSF project No. 19-11-00023 based on MIPT.
For citation: Maxim V. Muratov, Vasily V. Ryazanov, Igor B. Petrov. Inverse problems of macrofracture formations exploration seismology solution with use of convolutional neural networks. *RENSIT*, 2020, 12(2):253-262. DOI: 10.17725/rensit.2020.12.253.

Contents

1. INTRODUCTION

Currently, exploration seismology [1,2] is one of the most reliable methods for finding oil and gas deposits and preparing the rock before deep drilling. The ongoing research is aimed at determining the structure of geological

formations, as well as the possible location of the hydrocarbon field. Dense carbonate rocks and deep-lying sandstones account for an increasing share of exploration. Hydrocarbon-containing formations of such rocks are usually penetrated by systems of subvertical, uniformly oriented fractures of various scales, filled with liquid [3,4]. They determine the reservoir properties, being the basis for constructing models of fields to justify their development modes.

One of the founders of the theory of seismic migration was J. F. Claerbout [5,6]. With the advent of modern high-performance computing systems, considerable efforts have been made to develop new high-precision methods [7,8] for solving inverse seismic problems. Initially, all methods were based on an acoustic approach that did not take into account the influence of shear waves. To overcome this drawback, a two-wave elastic model was used [9]. Nowadays the great interest for seismologists is the identification of fractured zones. This is due to the high permeability of the medium and the potentially high content of hydrocarbons. Various mathematical models have been developed taking into account the complex structure of the geological medium [10-12]. Diffracted waves are in the process of a comprehensive study by exploration geophysicists. A large number of scientific papers are devoted to numerical modeling of seismic reactions from fractured media [13,14].

In recent years, machine learning methods, and in particular deep neural networks, have shown impressive results in many areas, such as computer vision, speech recognition, and machine translation. For example, in the field of computer vision, it was possible to solve many problems that were previously unsolved, such as the classification problem [15], the recognition problem [16], and the image generation problem [17].

One of the significant advantages of deep learning methods is that these methods can be transferred to many other areas related to the processing of large amounts of data. One such area is the task of seismic exploration. Several works in this area have already been carried out. In [18], the problem of detecting a fault in 2 dimensions using a deep convolutional neural network was solved. Synthetic data obtained by solving large direct problems were used as data for training the neural network. In [19], a similar problem was solved in 3 dimensions. The great advantage that is highlighted in these works is that the input data for deep learning algorithms do not require special processing and, therefore, such methods can be easier to use than standard seismic methods. Flexibility and relative simplicity make such methods effective to solve practical problems. So, in [20], deep neural networks are used to detect CO_2 emissions, and in [21], these methods are used to detect and classify defects in composite materials.

Formulation of the problem

In this paper, we consider the process of solving the inverse problem of exploration seismology of systems of unidirectional macrofractures (**Fig. 1**) using convolutional neural networks. The following notation is introduced in the figure: α – fracture inclination angle, h – the height of fractures, d – the distance between fractures (a parameter characterizing the density of fractures at a given horizontal extent of the system). The horizontal dimension in all experiments was considered constant and equal to 1000 m. The angle of inclination of

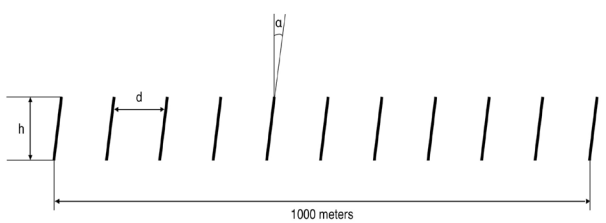

Fig. 1. *The scheme of macrofractures system.*

the fractures varied in the interval from -15° to +15° relative to vertical, the height of fractures varied from 50 to 200 m, the distance between fractures – from 50 to 200 m.

The training set was formed using mathematical modeling of direct two-dimensional problems using the grid-characteristic method on unstructured triangular meshes [22].

In the considered inverse problems, the elastic characteristics of the geological medium were considered known: longitudinal wave velocity 2250 m/s, transverse – 1250 m/s, the density of medium – 1180 kg/m^3. The system is placed in depth of 2000 m. A plane wave was excited on the surface of the earth, propagating deep into the geological medium. The response of the reflected and diffracted waves, which were formed when the incident wave front passed through the system of fractures, was recorded on seismic receivers located on the surface above the system of fractures with an interval of 50 m (100 receivers in total).

The problems in which the following parameters were varied were considered:

- the angle of inclination of the fractures;
- the height of the fractures;
- the angle of inclination and the height of the fractures at the same time;
- fracture density (distance between fractures);
- simultaneously, all three parameters - the angle, height and density of fractures.

Qualitatively, the influence of the height and distance between fractures on the response picture was described in [23].

2. MATERIALS AND METHODS

2.1. Methodology for direct problem solving

The determining equations system of a linearly elastic medium can be represented in the form [24]:

$$\rho\frac{\partial V_i}{\partial t}=\frac{\partial T_{ji}}{\partial x_j},\ \frac{\partial \mathrm{T_{ij}}}{\partial \mathrm{t}}=\lambda\left(\sum_k\frac{\partial V_k}{\partial x_k}\right)I_{ij}+\mu\left(\frac{\partial V_i}{\partial x_j}+\frac{\partial V_j}{\partial x_i}\right). \quad (1)$$

where V_i – the velocity component, T_{ji} – the stress tensor, ρ – the density of medium, λ and μ – the Lame coefficients, I_{ij} – the component of unit tensor. By entering the vector of variables $\vec{u}=\{V_x,V_y,T_{xx},T_{yy},T_{xy}\}$, the system (1) write as:

$$\frac{\partial\vec{u}}{\partial t}+\sum_{i=1,2}A_i\frac{\partial\vec{u}}{\partial\xi_i}=0. \quad (2)$$

The numerical solution of (2) is found using the grid-characteristic method [25]. We carry out coordinatewise splitting and by changing variables we reduce the system to a system of independent scalar transfer equations in Riemann invariants:

$$\frac{\partial\vec{w}}{\partial t}+\Omega_i\frac{\partial\vec{w}}{\partial\xi_i'}=0,\ \ i=1,2. \quad (3)$$

For each transfer equation (3), all nodes of the computational mesh are bypassed, and characteristics are omitted for each node. From the time layer n, the corresponding component of the vector $\vec{w}$ transfer to the time layer n+1 as

$$w_k^{n+1}(\xi'_i)=w_k^n(\xi'_i-\omega_k\tau),$$

where τ – the time step.

After all the values are transferred, we go to a reverse transition to the vector of the desired values $\vec{u}$.

The interpolation on unstructured triangular meshes is considered. Values at each point are found using values at mesh reference points $\vec{w}(\vec{r}_{ijkl})$ and their weights $p_{ijkl}(\vec{r})$ as:

$$\vec{w}(\vec{r})=\sum_{i,j,k,l}\vec{p}_{ijkl}(\vec{r})\,\vec{w}(\vec{r}_{ijkl}).$$

The grid-characteristic method allows the most correct algorithms to be applied at the boundaries and contact boundaries of the integration domain [26,27].

The boundary condition can be written in common view as:

$$\boldsymbol{D}\vec{u}(\xi_1,\xi_2,t+\tau)=\vec{d},$$

where $\mathbf{D}$ – some matrix 5×2, $\vec{d}$ – some vector, $\vec{u}(\xi_1,\xi_2,t+\tau)$ – the values of the desired

velocity components and the components of the stress tensor at the boundary point at the next time step.

2.2. Mathematical models of fractures

In real exploration seismology problems, one has to deal with heterogeneity in the nature of the interaction of elastic waves with the surface of a fracture as it passes through it. A fracture is a complex heterogeneous structure [4,28]. In places, the flaps of the fractures are at some distance and are separated by a saturating fluid or gas [28], in some points adhesion is observed, the walls are closely adjacent to each other under the action of pressure forces [29]. In addition, fractures can be classified according to the nature of saturation: fluid or gas [28, 29].

In the problem under consideration, discrete fractures models based on the concept of an infinitely thin fracture were used. The fracture was defined as a boundary or contact boundary with a certain boundary condition.

a) Gas-saturated fracture

The gas-saturated fracture model simulates well the behavior of fractures filled with air or gas at a shallow depth of 100-150 m [29]. At great depths, under the influence of pressure, fractures with air close, and gas acquires the properties of a liquid.

The fracture is defined as the boundary condition of free reflection on the flap flaps:
$\boldsymbol{T}\vec{n} = 0.$

b) Fluid-filled fracture

In most practical problems, fractures are filled with fluid: water, oil, liquefied gas, etc. [22,28,29] Therefore, it was advisable to develop a model to describe such a situation.

A fluid-filled fracture is defined as a contact boundary with the condition of free sliding [22]:

$$\vec{v}_a \cdot \vec{n} = \vec{v}_b \cdot \vec{n}, \;\; \vec{f}_n^{\,a} = -\vec{f}_n^{\,b}, \;\; \vec{f}_\tau^{\,a} = \vec{f}_\tau^{\,b} = 0.$$

Such a contact boundary completely transmits longitudinal vibrations without reflection and completely reflects transverse waves. Such a picture corresponds to the real situation: the values of the propagation velocities of longitudinal waves in liquids and densities are comparable with the values of velocities and densities of geological media; while the rates of transverse vibrations in liquids are close to zero.

c) Glued fracture

At great depths under the influence of pressure, it happens that the flaps of the fractures touch so that the elastic waves almost completely pass through the fracture. In this case, it will optimally use the contact condition of complete adhesion [22]:

$$\vec{v}_a = \vec{v}_b, \;\; \vec{f}_a = -\vec{f}_b,$$

where $\vec{v}$ are velocities of closed boundary points, $\vec{f}$ – the force acting to the boundary, *a* and *b* are the first and the second flaps of fracture.

d) Partially-glued fracture

In real exploration seismology, partially glued fractures can occur [22,29], in which part of the surface of the flaps is sticky and part is separated by a fluid or gas. Such fractures show partial transmission of the elastic wave front, which affects the amplitudes of the response waves in the seismograms.

A model of the fracture was developed, where at different points of the flaps the conditions of gas-saturation (fluid-filling) and complete adhesion were randomly set. The number of certain points was regulated by a weight coefficient – the coefficient of gluing. Such a model made it possible to specify gas-saturated and fluid-filled fractures with a percentage of sticking points from 0 to 100% percent.

2.3. The neural network structure

In all experiments, a similar neural network architecture was used. Samples were generated

during the solution of the direct problem, the structure of the objects supplied to the input of the neural network coincided, the set of target variables differed.

Each object was a set of measurements of the horizontal and vertical components of the velocity (V_x, V_z) of vibrations. Velocity data was obtained from a series of evenly spaced sensors and measured at equal time intervals.

Based on this, each sample was transformed into a three-dimensional object (velocity component, number of sensors, number of time measurements) of size (2, 100, 300), respectively (**Fig. 2**).

To predict the angle of inclination, a convolutional neural network was used. Convolutional networks have worked well in solving problems of classification, regression, segmentation, etc. on visual-, audio- and other data.

The convolutional network differs from other types of neural networks by the presence of convolutional and pooling layers. These layers can significantly reduce the number of network parameters, accelerate the speed of learning.

The following types of layers were used in the current task: convolutional layer, MaxPooling layer, fully connected layer. Experiments were carried out with the addition of Dropout layers, but their use impaired the accuracy of

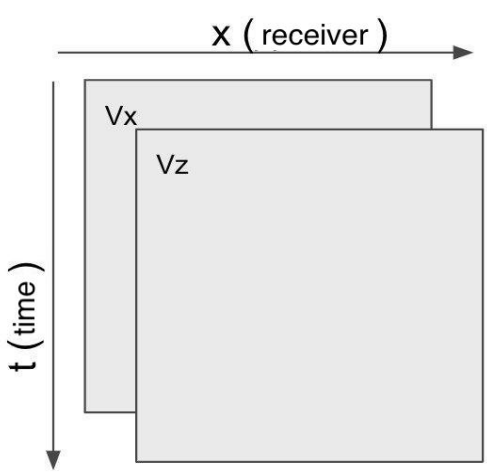

Fig. 2. *The scheme of learning and validation sets.*

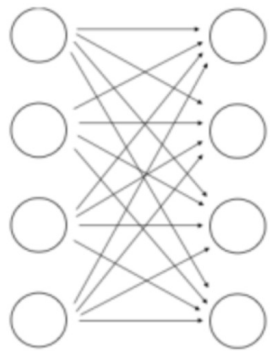

Fig. 3. *Fully connected layer.*

the predictions. Here is a brief description of each of the layers used.

a) Fully connected layer

The fully connected layer is a classic for most types of neural networks. In this layer, each neuron from the previous layer is connected to the neuron of the next layer (**Fig. 3**). Layers of this group are used in many types of tasks: their advantage is that they take into account the maximum amount of information and connections between neurons. The disadvantage is the large number of parameters, which is equal to the number of edges in conjunction with the number of output neurons. Another drawback is the fact that a large number of parameters can degrade the convergence of the optimized function.

b) Convolutional layer

Convolutional layers are a characteristic feature of the convolutional neural network (**Fig. 4**). Their feature is that instead of pairwise combining of outgoing and incoming neurons,

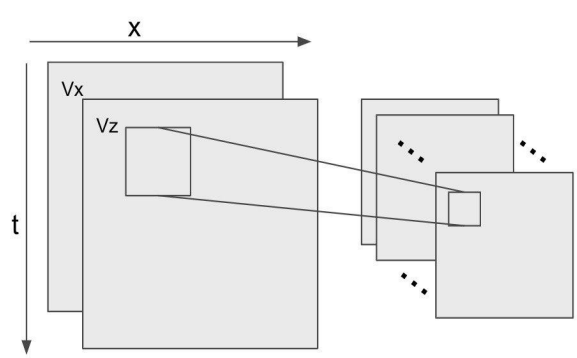

Fig. 4. *Convolutional layer.*

only certain local neurons are combined. The next feature is the joint use of the same scales for different ribs, which speeds up and simplifies training. For clarity, the convolutional layer scheme can be represented in the form of a filter sliding along the selected axes (there can be 1,2,3 or more). One filter passes through all possible points and forms the next level of neurons by scalar multiplication of the filter values by the values of the object. The number of parameters is equal to the product of the number of filters and the filter size. During the current experiments, two-dimensional convolutional layers were used, in which one axis corresponded to the measurement time and the second to the position of the sensor. Thus, a two-dimensional map of signals is created.

As the advantages of this type of layers it should be noted a small number of parameters that are limited by the size of the filter, the sharing of weights. These factors accelerate the training of the neural network and find specific features of objects along the indicated axes. It is these features that make convolutional neural networks very popular for solving pattern recognition tasks (2 axes - width and height of the image), text analysis (1 axis - letter / word position in the text) or audio (one axis - time, or two axes - time and sound frequency)

Of the disadvantages - the use of this type of layer is limited to certain types of tasks.

c) MaxPooling layers

MaxPooling (also called AveragePooling) layers are also typical for convolutional neural networks. These layers are nonparametric, and their work is to select the maximum (or average) value inside the given window and transfer this value to the neuron of the next layer (**Fig. 5**). Pooling layers allow us to reduce the number of neurons in the next word 4 (9, 16, ...) times, thereby reducing the number of

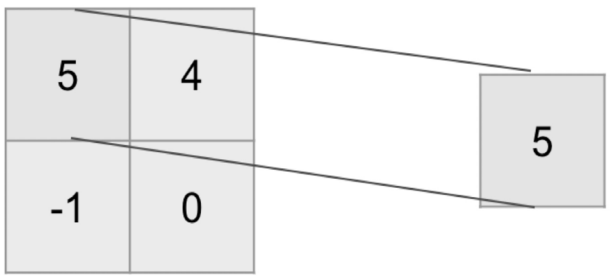

Fig. 5. *MaxPooling layer.*

weights on the next layers. In practice, these types of layers are almost universally used in the training of convolutional neural networks to improve their convergence.

In neural networks, output signals from neurons pass through a non-linear activation function. Examples include hyperbolic tangent, sigmoid, ReLU (Restricted Linear Unit, function of the form $y = \max(0, x)$). Without activation functions, a neural network (or a subset of its layers) would turn into a simple linear function, so the presence of nonlinear activations is an essential component of a neural network. The choice of activation function is left to the discretion of the researcher. In this work, we used the ReLU activation function, the graph of which is shown in **Fig. 6**.

The general view of the neural network used for the above experiments can be described as follows:

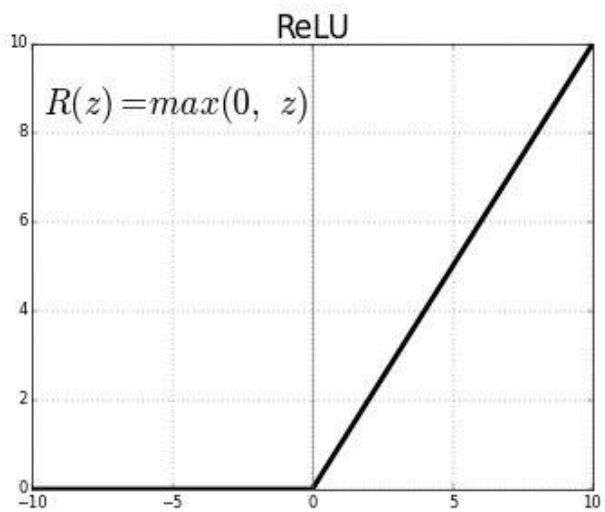

Fig. 6. *The graph of activation function ReLU.*

1. Convolutional layer (32 filters (cores), 3×3 core size, ReLU activation function)
2. MaxPooling layer (size 2×2, without activation function)
3. Convolutional layer (32 cores, 3×3 kernel size, ReLU activation function)
4. MaxPooling layer (size 2×2, without activation function)
5. Fully connected layer (64 neurons, ReLU activation function)
6. The output layer (1,2,3 neurons depending on the task)

The output layer for the problems under consideration was different. In the case of the angle of inclination, thickness, density - one neuron, the angle of inclination and thickness - two neurons, all parameters are three neurons. As a loss function (loss function), the value Mean Squared Error (MSE, root mean square error) was used. During the training, the Mean Absolute Error metric (MAE, average modulo error) was also monitored. These metrics can be used both for a one-dimensional quantity and for multidimensional vectors

$$MAE = \frac{1}{N}\sum_{i=1}^{N}|y_i - \hat{y}|, \quad MSE = \frac{1}{N}\sum_{i=1}^{N}(y_i - \hat{y})^2.$$

Neural network training

The neural network was trained in 32 mini-batches. The Adam optimization algorithm (adaptive moment estimation) was chosen. This optimization algorithm has many advantages (low memory requirements, simple and computationally efficient). The Adam algorithm is different from the classical stochastic gradient descent methods, which maintain a constant training speed during training to update weights. In the Adam algorithm, the training rate is updated taking into account the estimates of the first and second moment. This algorithm is well established for optimization of regression problems by neural networks. In these experiments, the initial convergence rate was set to 0.001.

3. RESULTS

The neural network was trained and validation was carried out on sets of solutions of the direct problem for the tasks with variations: the angle of inclination of the fractures, the height of the fractures, the angle of inclination and height at the same time, the density of the location of the fractures (the distance between them) and all three parameters at the same time.

Angle of inclination

For the problem with a variation in the angle of inclination of fractures in the system in the range from -15 to +15 degrees relative to the vertical (subvertical fractures), training was performed on a set of 4021 solutions of the direct problem and then validation was performed on a set of 1981 control samples. **Fig. 7** shows a graph of the dependence of the average error in recognition on the epoch of training (32 epochs in total). It can be seen that a sufficiently low error is achieved – less than 1%.

Height of fractures

For a problem with a variation in the height of fractures in a system in the range from 50 to 200 meters, training was performed on a set of 4018 solutions to the direct problem and then validation was performed on a set of 1980 control samples. **Fig. 8** shows a graph of the

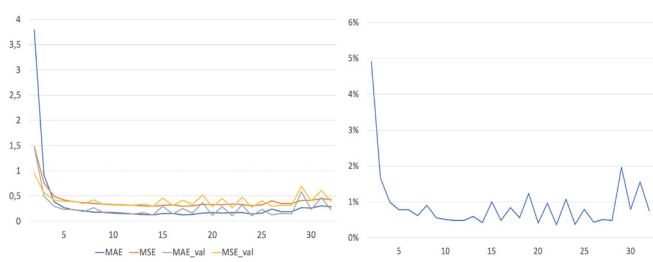

a *b*

Fig. 7. *Graphs of the metrics MAE and MSE depending on the number of the training epoch (a) for the training (MAE, MSE) and validation (MAE_val, MSE_val) sets with varying angles. Dependence of the error in determining the angle of inclination of fractures on the number of the epoch of training (b).*

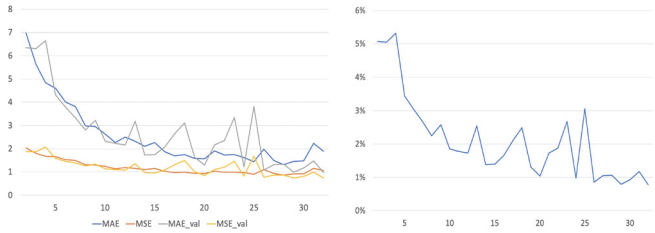

a *b*

Fig. 8. *Graphs of the metrics MAE and MSE depending on the number of the training epoch (a) for the training (MAE, MSE) and validation (MAE_val, MSE_val) sets with varying fracture heights. The dependence of the error in determining the height of fractures on the number of the epoch of training (b).*

dependence of the average error in recognition on the epoch of training (32 epochs in total). It can be seen that a sufficiently low error is achieved - about 1%.

Simultaneous variation in inclination and fracture height

For the problem with simultaneous variation of the angle of inclination of fractures in the system in the range from -15 to +15 degrees relative to the vertical (subvertical fractures) and the height of fractures in the system in the range from 50 to 200 meters, training was conducted on a set of 4020 solutions of the direct problem and then validation was performed on a set of 1981 control samples. The **Fig. 9** shows a graph of the dependence of the average error in recognition on the

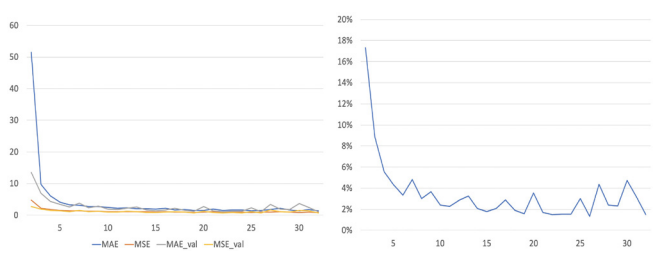

a *b*

Fig. 9. *Graphs of the MAE and MSE metrics depending on the number of the training epoch (a) for the training (MAE, MSE) and validation (MAE_val, MSE_val) sets with variation in the angle and fracture height. The dependence of the error in determining the angle of inclination and the height of the fractures on the number of the training epoch (b).*

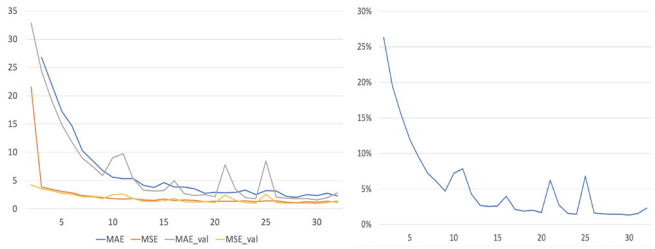

a *b*

Fig. 10. *Graphs of the MAE and MSE metrics depending on the number of the training epoch (a) for the training (MAE, MSE) and validation (MAE_val, MSE_val) sets with varying fracture densities. Dependence of the error in determining the density of the location of fractures on the number of the training epoch (b).*

epoch of training (total 32 epochs). It can be seen that a sufficiently low error is achieved - about 3-4%.

Fracture density (the distance between fractures in system)

For a problem with a variation in the density of fractures (distance between fractures) in a system in the range from 50 to 200 meters, training was conducted on a set of 3350 solutions of the direct problem and then validation was performed on a set of 1650 control samples. **Fig. 10** shows a graph of the dependence of the average error in recognition on the epoch of training (a total of 32 epochs). It can be seen that a sufficiently low error is achieved - about 2%.

Simultaneous variation of all three parameters

For a problem with simultaneous variation of the angle of inclination of fractures in the system in the range from -15 to +15 degrees relative to the vertical (subvertical fractures), the height of fractures in the system in the range of 50 to 200 meters and the density of fractures (distance between fractures) in the system in the range of from 50 to 200 meters, training was conducted on a set of 4020 solutions of the direct problem, and then validation was performed on a set of 1981 control samples. **Fig. 11** shows a graph of the

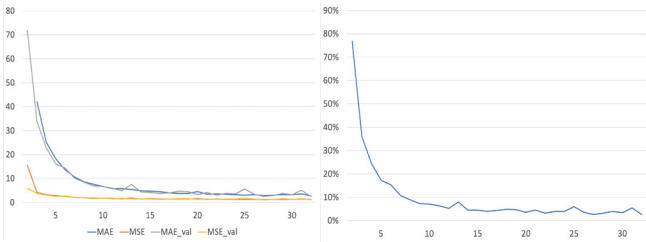

a *b*

Fig. 11. *Graphs of the metrics MAE and MSE depending on the number of the training epoch (a) for the training (MAE, MSE) and validation (MAE_val, MSE_val) sets when all three parameters are varied. The dependence of the error in determining the angle of inclination, height and density of the location of fractures on the number of the epoch of training (b).*

dependence of the average error in recognition on the epoch of training (32 epochs in total). It can be seen that a sufficiently low error is achieved - about 5-7%.

4. CONCLUSION

The research showed good applicability for solving the inverse problems of exploration seismology of macrofractures layers of machine learning techniques, in particular convolutional neural networks, with training sets obtained by solving direct problems by mathematical modeling using the grid-characteristic method. In the most complicated formulation — when varying the three main parameters of a unidirectional fracture system (inclination angle, height and fracture density) — we got a recognition error of only 5-7%, which is a fairly good indicator.

Low error indices make it possible to complicate the task by introducing additional parameters for variation (for example, the spatial position of the system of fractures, as was done for a single fracture in [30]). What will be done in further research.

REFERENCES

1. Sheriff RE, Geldart LP. *Exploration seismology.* Cambridge University Press, 1995, 592 p.
2. Braduchan YuV, Goldberg AV, Gurari FG. *Bazhenovskii gorizont Zapadnoi Sibiri* [Bazhen horizon of West Siberia]. Novosibirsk, Nauka Publ., 1986, 216 p.
3. Dorofeeva EV. *Tektonicheskaya treschinovatost' gornykh porod i usloviya formirovaniya treschinnykh kollektorov nefti i gaza* [Tectonic fracturing of rocks and conditions for the formation of fractured reservoirs of oil and gas]. Moscow, Nedra Publ., 1986, 231 p.
4. Kozlov EA. *Modeli sredy v razvedochnoi seismologii* [Models of medium in exploration seismology]. Tver, GERS Publ., 2006, 480 p.
5. Claerbout JF. Coarse grid calculations of waves in inhomogeneous media with application to delineation of complicated seismic structure. *Geophysics*, 1970, 36(3):407-418.
6. Claerbout JF, Doherty SM. Downward continuation of moveout-corrected seismograms. *Geophysics*, 1972, 37(5):741-768.
7. Etgen J, Gray S, Zhang Y. An overview of depth imaging in exploration geophysics. *Geophysics*, 2009, 74:WCA5-WCA17.
8. Jiao K, Huang W, Vigh D, Kapoor J, Coates R, Starr EW, Cheng X. Elastic migration for improving salt and subsalt imaging and inversion. *SEG Technical Program Expanded Abstracts,* 2012, 1-5.
9. Luo Y, Tromp J, Denel B, Calandra H. 3D coupled acoustic-elastic migration with topography and bathymetry based on spectral-element and adjoint methods. *Geophysics*, 2013, 78(4):S193-S202.
10. Burago NG, Nikitin IS, Yakushev VL. Hybrid Numerical Method with Adaptive Overlapping Meshes for Solving Nonstationary Problems in Continuum Mechanics. *Computational Mathematics and Mathematical Physics*, 2016, 56(6):1065-1074.
11. Nikitin IS, Burago NG, Nikitin AD. Explicit-Implicit schemes for solving the problems of the dynamics of isotropic and anisotropic elastoviscoplastic media. *IOP Conf. Series: Journal of Physics: Conf. Series*, 2019, 1158(3):1-8.
12. Burago NG, Nikitin IS. Algorithms of through calculation for damage processes. *Computer Research and Modeling*, 2018, 10(5):645-666.
13. Fang X, Zheng Y, Fehler MC. Fracture clustering effect on amplitude variation with

offset and azimuth analyses. *Geophysics*, 2017, 82(1):N13-N25.

14. Muratov MV, Petrov IB. Application of fractures mathematical models in exploration seismology problems modeling. *Smart Innovation, Systems and Technologies,* 2019, 120-131.
15. Krizhevsky A, Sustskever I, Hinton GE. Imagenet classification with deep convolutional neural networks. *Advances in neural information processing systems*, 2012, 1097-1105.
16. Szegedy C, Toshev A, Erhan D. Deep neural networks for object detection. *Proc. of the 26th Intern. Conf. on Neural Information Processing Systems* (*NIPS'13*), 2013, 2:2553-2561.
17. Goodfellow I, Pouget-Abadie J, Mirza M, Xu B, Warde-Farley D, Ozair S, Courville A, Bengio Y. Generative adversarial nets. *Advances in neural information processing systems*, 2014, 2672-2680.
18. Zhang C, Frogner C, Araya-Polo M, Hohl D. Machine-learning Based Automated Fault Detection in Seismic Traces. *EAGE Conference and Exhibition,* 2014.
19. Araya-Polo M, Dahlke T, Frogner C, Zhang C, Poggio T, Hohl D. Automated fault detection without seismic processing. *The leading edge,* 2017, 36(3):194-280.
20. Wu Yu, Lin Yo, Zhou Zh, Delorey A. Seismic-Net: A Deep Densely Connected Neural Network to Detect Seismic Events. *CoRR,* 2018.
21. Menga M, Chua YJ, Woutersonb E, Ong CPK. Ultrasonic signal classification and imaging system for composite materials via deep convolutional neural networks. *Neurocomputing*, 2017, 257:128-135.
22. Petrov IB, Muratov MV. The application of grid-characteristic method in solution of fractured formations exploration seismology direct problems (review article). *Matem. Mod.*, 2019, 31(4):33-56.
23. Leviant VB, Petrov IB, Muratov MV. Chislennoe modelirovanie volnovikh otklikov ot sistemy (klastera) subvertikalnykh makrotreschin [Numerical simulation of wave responses from subvertical macrofractures system]. *Technologii seismorazvedki*, 2012, 1:5-21 (in Russ.).
24. Novatskii VK. *Teoriya uprugosti* [Elastic theory]. Moscow, Mir Publ., 1975, 872 p.
25. Magomedov KM, Kholodov AS. *Setochno-kharakteristicheskie chislennye metody* [Grid-characteristic numerical methods]. Moscow, Nauka Publ., 1988, 288 p.
26. Petrov IB, Tormasov AG, Kholodov AS. On the use of hybrid grid-characteristic schemes for the numerical solution of three-dimensional problems in the dynamics of a deformable solid. *USSR Computational Mathematics and Mathematical Physics*, 1990, 30(4):191-196.
27. Favorskaya AV, Breus AV, Galitskii BV. Application of the grid-characteristic method to the seismic isolation model. *Smart Innovation, Systems and Technologies*, 2019, 133:167-181.
28. Leviant VB, Petrov IB, Kvasov IE. Chislennoe modelirovanie volnovogo otklika ot subvertikalnykh makrotreschin, veroyatnykh fluidoprovodyaschikh kanalov [Numerical modeling of seismic response from subvertical macrofractures as possible fluid conduids]. *Tekhnologii seismorazvedki*, 2011, 4:41-61 (in Russ.).
29. Leviant VB, Miryakha VA, Muratov MV, Petrov IB. Otsenka vliyaniya na seismicheskii otklik raskrytosti treschiny i doli ploschadi lokalnykh kontaktov k ee poverkhnosti [Seismic responses of vertical fractures depending on their thickness]. *Tekhnologii seismorazvedki,* 2015, 3:16-30 (in Russ.).
30. Muratov MV, Biryukov VA, Petrov IB. Solution of the Fracture Detection Problem by Machine Learning Methods. *Doklady Mathematics*, 2020, 101(2):169-171.